# OBSERVATION OF THE DIURNAL VARIATION OF UPPER TROPOSPHERIC DIVERGENCE IN A TROPICAL CONVECTIVE SYSTEM

Johannes Schmetz, Kenneth Holmlund,
Marianne König and Hans-Joachim Lutz

EUMETSAT, D-64295 Darmstadt, Germany

ABSTRACT

The paper studies the diurnal variation of divergence of the upper level wind field of a tropical deep convective system and the simultaneous development of cloud cover, cloud height, upper tropospheric humidity (UTH) and outgoing longwave radiation (OLR). The wind field is derived from the tracking of cloud and water vapour features observed by Meteosat-7 in the water vapour channel (WV: 5.7 – 7.1 μm). The analysis shows a diurnal cycle of divergence with values ranging from 2 to about $10.10^{-5}$ $s^{-1}$. Analysis of cloud cover, mean brightness temperature of the coldest 2% of clouds, OLR and UTH show a distinct relationship with the convective activity as described by the upper level divergence: Relative to the peak in convective activity (05:30 to 07:00 UTC) the high level cloud cover reaches a maximum 6 – 7 hours later. The maximum of UTH lags nearly 12 hours behind and the minimum of OLR is reached after 8 – 9 hours. The analysis also supports the existence of a barrier to vertical mixing at 13 – 14 km.

## 1 Introduction

Diurnal cycles of deep convective tropical cloud systems are commonly observed. Those diurnal cycle are most pronounced over the continents and most often forced by the daily course of the solar surface heating. Typically the diurnal cycle of convective systems over land leads to minima of the OLR in the afternoon and early evening which is asscociated with a maximum in precipitation (e.g. Gray and Jacobson, 1977; Hendon and Woodberry, 1993). Previous satellite studies of the diurnal cycle mainly addressed clouds only and were based on thermal IR window channel observations. The diurnal variation of the Upper Tropospheric Humidity (UTH) can also be documented with help of the water vapour (WV) channel, although few studies have dealt with this problem. Notably Udelhofen and Hartmann (1992) and Soden (2000) examined the diurnal variations in the UTH and studied the diurnal relationships between cloudiness, convection and water vapour; those studies will be used as reference for comparison.

This paper presents a single case study of the diurnal development of a deep convective tropical cloud system. Various geophysical parameters are analysed. A novel aspect is the direct estimate of the upper level wind divergence field from satellite derived atmospheric motion vectors (AMV).

## 2 Data Analysis

The case study uses images from the IR (10.5 – 12.5 μm) and water vapour channel (WV: 5.7 – 7.1 μm) of Meteosat-7. The chosen area extends from 4° N – 6° S and 12° E – 22° E over central Africa corresponding to about 1200km x 1200km represented by more than 50000 pixels. Data are for 28 June 1999 and, in addition to the satellite data, ECMWF analysis data have been used as auxiliary data for cloud analysis and UTH analysis. The following subsections explain how the geophysical parameters are derived.

## 2.1 Wind Field and Divergence

Winds have been derived from the WV channel, using the Meteosat Second Generation (MSG) prototype algorithm, described in more detail by Holmlund (2000). The vectors are derived with a cross-correlation technique using a 24x24 pixel template and searching in a area of 16x16 pixels. Overlap has been confined to 30% of the area in order to avoid tracking of the same feature. The wind fields are quality controlled following Holmlund (1998) and vectors with are quality indicator (QI) higher than 0.2 are retained.
Earlier work has shown that it is difficult to infer divergence fields directly from the wind vectors since the differentiation amplified the noisy character of the wind field; e.g. Schmetz et al. (1995) used monthly averages of divergence fields in order to reduce the noise. In order to derive instantaneous divergence fields from the AMV field, a QI-weighted Barnes filter has been run over the wind vectors before computing the divergence with finite differences over areas of 3x3 pixels as described in Holmlund (2000). The weights are computed from:

$$w = \exp\left[ -\left(\frac{\Delta r}{r_o}\right)^2 - \left(\frac{\Delta t}{t_o}\right)^2 - \left(\frac{1-qi}{qi_o}\right)^2 \right] \quad (1)$$

with $r_o$ = 2° lat/long; $t_o$ = 0.5 h; $qi_o$ = 0.4. $\Delta t$ is set to zero here.

Figure 1 shows the time series of the divergence (solid line with asterisks) as a function of time. The divergence increases from values around $3.10^{-5}$ $s^{-1}$ to more than $10.10^{-5}$ $s^{-1}$ over the course of 6 hours. Then the divergence decreases rapidly and later more gradually to values of $2.10^{-5}$ $s^{-1}$. The AMVs have been derived from nominal scans with intervals of 30 minutes. The divergence values refer to the maxima observed in the 'Barnes-interpolated' field. This is important, as it means that divergence values are representative of a scale of a few 100 km and that the approach is approximately Lagrangian, because the maximum value moves with time and is followed by the analysis.
For the period between 0900hUT and 1800h UT rapid scans were available with time intervals of 7.5 minutes; wind fields derived from rapid scans seem to provide slightly higher divergence values. However, this result is not considered conclusive and warrants further study. The main result is that the deep convective system reaches a maximum upper level divergence around 0630h. Therefore it should be is noted that this convective system is not driven by solar surface forcing as most commonly observed over tropical land areas.

It is also interesting that the kinematic vertical velocity can be estimated from the divergence. At a given point the change in vertical velocity $d\omega$ can be related to the horizontal divergence by:

$$d\omega = - \nabla \cdot \vec{v}\, dp \quad (2)$$

Assuming that the divergence flow is between pressure level p and p', integration leads to:

$$\omega(p) = \omega(p') - \int_{p'}^{p} \nabla \cdot \vec{v}\, dp \quad (3)$$

With the assumed boundary condition $\omega(p' = 100\,hPa) = 0$

one can compute a vertical velocity at 300 hPa. Taking the range of the divergence values in Figure 1 yields mean vertical velocities between 14 and 70 hPa/h, which is quite a realistic value for a tropical convective system of this scale. It is important to note that the actual height of the observed divergence increases with cloud top height. The fact that a divergence can be observed before the cloud system reaches the tropopause layer also indicates that the process of ambient moistening operates continuously while the cloud top rises through the upper troposphere observed by the WV channel. This issue requires deeper study in the future.

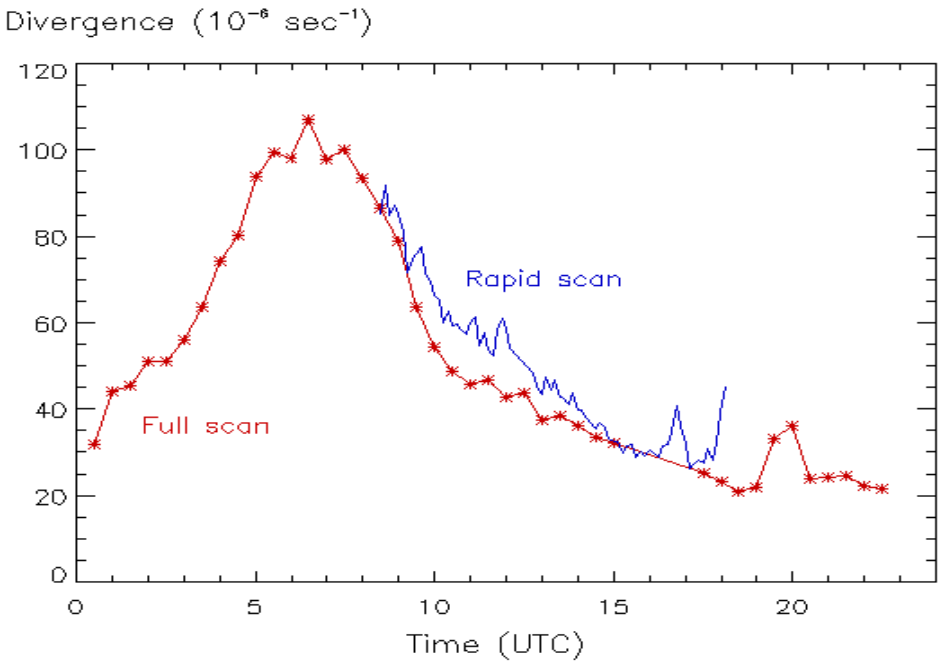


Figure 1: Divergence field computed from Atmospheric Motion Vectors (AMV) for the deep convective system. Note that the Figure shows the maximum of the divergence field, the position of which moves in location with time. The line denoted with asterisks shows the results for normal full disk scan (30 minutes). The solid line the results from rapid scans with 7.5 minute intervals. The area is over the Africa continent from 4°N – 6°N and 12°E – 22°E. Date is 28 June 1999

## 2.2 Cloud Parameters

Cloud parameters have been derived with the prototype algorithms developed for Meteosat Second Generation (Lutz, 1999). The algorithm uses a hierarchy of threshold tests that have been tuned for application to Meteosat-7. Figure 2 shows the diurnal variation of high level cloud cover above 400 hPa and the total cloud cover. Most interesting here is the high level cloud cover that reaches its maximum around 1400h – 1600h UT, i.e. about 8 – 10 hours after the maximum in divergence.

Figure 3 shows the equivalent blackbody brightness temperature ($T_{IR}$) derived from the coldest 2%, 5% and 10% of the IR pixels. A minimum is observed around 0530h to 0600h thus well coinciding with the maximum in divergence although $T_{IR}$ seem to lead the divergence maximum by a short period. The specific form of the minimum – with a slight dip – is of some interest and gives rise to a speculation concerning a penetration of tropospheric air into the tropical transition layer above ~ 14 km height. This is better illustrated when the $T_{IR}$ based on the coldest 2 % of pixels, is transformed to geometric cloud top heights using corresponding ECMWF temperature analyses as plotted in Figure 4. Figure 4 shows a steady rise in cloud top temperature between 0000h and 0200h followed by constant cloud top of 14.3 km until about 0500h when another increase to about 14.7 km occurs. This is likely to be an example of deep convection that gets slowed down when it hits the barrier to vertical mixing around 14 km (Folkins et al., 1999). This height is the level where the general outflow occurs. It can be anticipated on thermodynamic reasoning, as it is the level at which the potential temperature becomes equal to the highest equivalent potential temperatures in the tropical boundary layer (c.f. Peixoto and Oort, 1992). Around 0430h – 0500h convection penetrates by about 400 m into the 'tropical tropopause layer' (TTL) (e.g. Gettelman et al. 2001).

This picture is corroborated by Figure 5, which shows a plot of pixels with equivalent blackbody temperatures $T_{WV}$ from the WV channel exceeding $T_{IR}$. As shown by Schmetz et al. (1997), in

situations where cloud tops reach the tropopause, or more correctly the bottom of the tropopause layer, $T_{WV}$ becomes larger than $T_{IR}$ . The number of pixels, for which $T_{WV} > T_{IR}$, provides a useful proxy for deep convective clouds. Figure 5 shows that between 0200h and 0400h the number of those pixels nearly doubles which is interpreted as a 'pushing of clouds against the bottom of the TTL', until 0430h – 0500h when penetration into the TTL occurs.

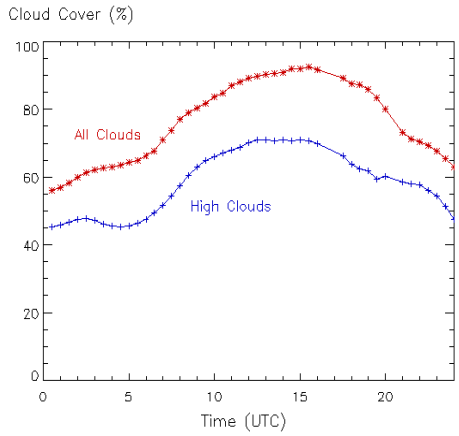


Figure 2: Total and high cloud over the area of the deep convective system. Area as in figure 1.

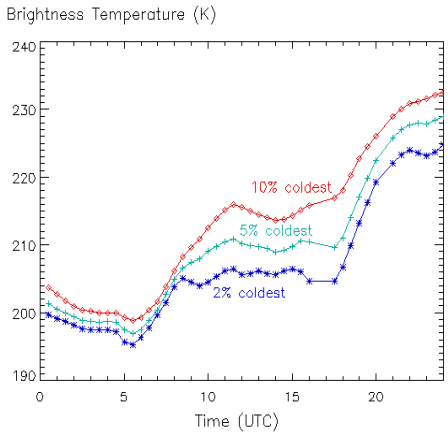


Figure 3: Mean IR brightness temperature of the coldest 2, 5 and 10%, of the cloudy pixels as function of time.

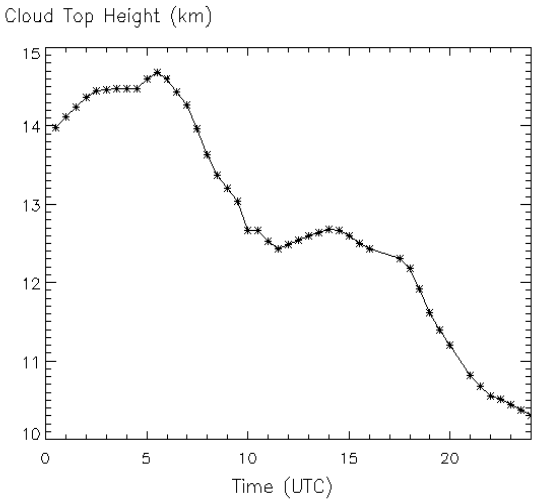


Figure 4: Cloud top temperature inferred from mean IR brightness temperatures $T_{IR}$ of the coldest 2 % of cloudy pixels. The nearest ECMWF analysis temperature profile has been taken to allocate cloud tops to a geometric height.

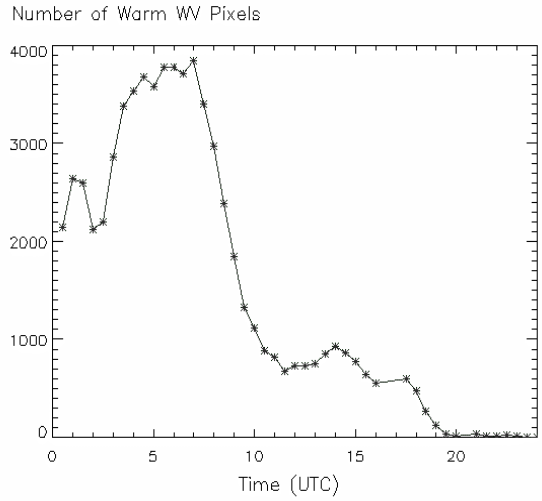


Figure 5: Number of WV pixels with $T_{WV} > T_{IR}$. Those pixel are a good proxy for deep convective clouds.

## 2.3 Upper Tropospheric Humidity (UTH)

Figure 6 shows the upper tropospheric humidity (UTH) as inferred with an algorithm described by Schmetz et al. (1995). The UTH represents a deep layer mean relative humidity defined with regard to liquid water (not ice). It starts increasing with the onset of convective outflow and the time of the maximum of upper level divergence divergence (see Figure 1). The maximum is reached around 1800h. Interesting is the slight decrease between 0400h and 0630, i.e. just before the divergence maximum. This could be explained by enhanced drying of clear sky pixels due to subsidence compensating the convective lifting. Indeed a closer examination of satellite pictures clearly shows this feature in proximity to the convective cloud system. It is noted however, that this observations is only qualitative because the UTH has been computed for the fixed geographical area and no attempt has been made for the to follow the cloud system and the associated subsiding area around.
The second curve in Figure 6 shows the number of clear sky pixels used to infer the UTH. The minimum of about 25000 pixels (out of about 55000) is reached at 1600h.

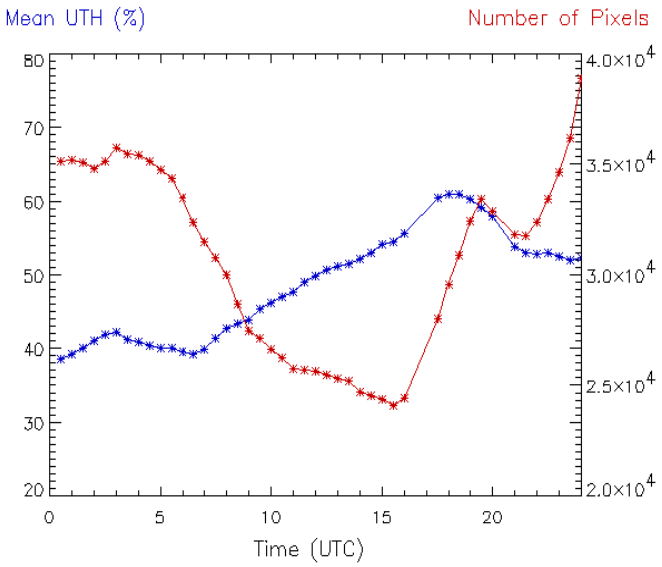


Figure 6: Cycle of mean Upper Tropospheric Humidity (UTH, blue) and number of clear sky pixels (right ordinate, red) used to infer the mean UTH.

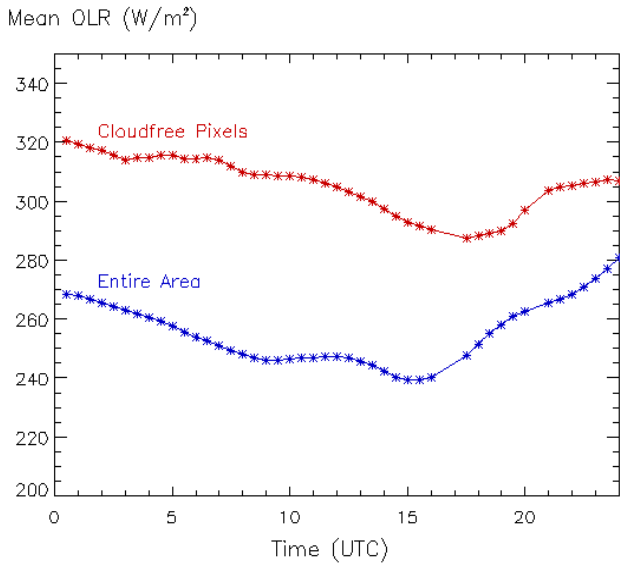


Figure 7: Mean Outgoing Longwave Radiative Flux (OLR) for the clear sky (red) and entire area (blue), respectively.

## 2.4 Outgoing Longwave Radiation (OLR)

The OLR has been estimated from the radiance observations in the IR and WV channel of Meteosat-7 using the regression technique of Schmetz and Liu (1988) with newly computed regression coefficients for Meteosat-7. Figure 7 shows the OLR derived for the entire area and the clear sky area, respectively. The mean OLR for the entire area has a minimum at 1500h while the clear sky OLR lags nearly 3 hours behind. This could be explained by two effects: i) the clear sky OLR decreases due to a detrainment of moist air from cloudy regions and ii) it also decreases due to an evaporation of cloud particles leaving behind a moistened clear atmosphere. The latter effect appears to be the dominating one, as can be inferred from Figure 6 which shows a steep increase of the number of clear sky pixels over the period from 1600h to 2000h UT.
In the near future, this kind of analysis will benefit from the simultaneous radiance and radiation budget observations from Meteosat Second Generation (MSG) (Schmetz et al., 2002). The dedicated Geostationary Earth Radiation Budget experiment (GERB) will provide radiation budget measurements that are independent from the detailed cloud and humidity information from the multispectral imager (SEVIRI) on board of MSG.

## 3 Synopsis of Results and Concluding Remarks

Table 1 summarises the seven geophysical parameters that have been analysed for this case study of a deep convective system over Central Africa. The second column gives the time of observed minima/maxima and the right column provides some additional observations on e.g. secondary extrema that can be physically explained.
The main conclusions from this preliminary study can be summarised as follows:

- Upper level wind field divergence in tropical deep convective system can be estimated directly from atmospheric motion vectors inferred from WV channel observations. Kinematic vertical velocities inferred from the wind field divergence reach values higher than 0.5 m/s on a scale of several hundred kilometers. Further work is needed to study the uncertainties in vertical velocity due to errors in the wind field and due to assumptions on the thickness of the divergence layer. The diurnal cycle of divergence range from $2 \cdot 10^{-5}$ $s^{-1}$ to $10 \cdot 10^{-5}$ $s^{-1}$. An issue requiring further study is the obvious variation of the altitude of the observed divergence field that rises with cloud top. The fact that a divergent flow is observed while the cloud top height increases, is indicative of a continuous moistening of the upper troposphere. The maximum outflow is reached when the cloud top reaches the tropopause layer.

- The maximum of convective activity around 06:30 h UT, as suggested by the divergence is generally supported by other measures of convective activity, such as the mean brightness temperature $T_{IR}$ of the coldest 2 % of pixels, and the number of pixels with $T_{wv} > T_{IR}$. However, the different maxima do not exactly coincide.

- The UTH has a maximum at 18:00 h, thus lagging the maximum in convective activity by about 12 h; certainly this requires further study. For comparison, Udelhofen and Hartmann (1992) found a time lag of ~ 8 hours in a study based on four days, while Soden (2000) finds a lag of about 4 hours. As shown by Soden (2000), using 3 months of data, sample size of the data does explain some of the discrepancy.

- The clear sky outgoing longwave radiation (OLR) in the surrounding area decrease from about 320 $Wm^{-2}$ at the time of peak convective activity to 290 $Wm^{-2}$ some 12 hours later. An interesting notion is to interpret this as a 'cloud induced humidity forcing' rather an integral part of cloud radiative forcing. This concept may serve as a useful and stringent test of climate simulation models.

- A simultaneous analysis of cloud top height and the number of pixels with $T_{wv} > T_{IR}$, indicates the existence of a barrier around an altitude of 14 km. This barrier inhibits the rising of cloud top for about 2 hours, which is then followed by penetration into the tropical tropopause layer. This issue warrants further analysis and will be addressed in future case studies.

- An important application of detailed observations of diurnal variability is the comparison with General Circulation Models (GCM) (Lin et al, 2000). Future observations from Meteosat Second Generation (Schmetz et al., 2002) will provide even more detailed observations of cloud development, cloud microphysics, humidity fields and radiation budget components, respectively, that could serve as stringent test data for GCM validation.

| **Parameter** | **Time of observed Maximum/Minimum (UTC)** | **Other Observations** |
|---|---|---|
| Divergence | 06:30 max | |
| High level cloud cover | 14:00 max | Weak relative minimum ~ 05:00 UTC |
| $T_{IR}$ of coldest 2% of pixels | 05:30 max | Rapid decrease from 195 k to 204 k within ~ 3 hours |
| Cloud top height | 05:30 max | Rapid decrease from 14.7 km to 12.3 km within ~ 3 hours, then fairly stable for ~ 6 hours |
| Pixels with $T_{WV} > T_{IR}$ | 07:00 max | Rapid decrease to ~ 25% of number of pixels within 3 hours |
| UTH | 18:00 max | Weak relative minimum at 06:30 UTC due to compensating subsidence |
| OLR | 15:00 min | Clear sky OLR has minimum around 18:00 UTC |

Table 1: Synopsis of the occurrence of extrema for the different geophysical parameters under study. The study area extends from4° N – 6° S and 12° E – 22° E and contains a rapidly developing convective system.

REFERENCES


Dessler, A.E., 2002: The effect of deep, tropical convection on the tropical tropopause layer, J. Geophys. Res., 107, D3,

Folkins, I., M. Loewenstein, J. Podolske, S.J. Oltmans and M. Proffitt, 1999: A barrier to vertical mixing at 14 km in the tropics: Evidence from ozone sondes and aircraft measurements. J. Geophys. Res., 104, D18, 22095 – 22102.

Gettelman, A., M.L. Salby, W.J. Randel and F. Sassi, 2001: Convection in the Tropical Tropopause Region and Stratosphere-Troposhere Exchange. SPARC newsletter n°17, 22 – 25.

Gray, W.M. and R.W. Jacobson, 1977: Diurnal variation of deep cumulus convection. Mon. Wea. Rev., 105, 1171-1188.

Hendon, H.H. and K. Woodberry, 1993: The diurnal cycle of tropical convection. J. Geophys. Res., 98, D9, 16623 – 16637.

Holmlund, K., 1998: The utilization of statistical properties of satellite-derived atmospheric motion vectors to derive quality indicators. Wea. Forecasting, 13, 1093 – 1104.

Holmlund, K., 2000a: The Atmospheric Motion Vector retrieval scheme for Meteosat Second Generation. Proc. Fifth Int. Winds Workshop, Lorne, Australia, EUMETSAT, EUM-P28, 201-208.

Holmlund, K., 2000b: The use of Observations error as an extension to Barnes interpolation scheme to derive smooth instantaneous vector fields from satellite-derived Atmospheric Motion Vectors. Proceedings of the 5th International Winds Workshop, Lorne, Australia.

Lin, X., D.A. Randall and L.D. Fowler, 2000: Diurnal Variablility of the Hydrologic Cycle and Radiative Fluxes: Comparisons between Observations and a GCM. Bull. Amer. Meteor. Soc., 4159 – 4179.

Lutz, H.J., 1999: Cloud processing for Meteosat Second Generation. EUMETSAT Tech. Department Tech. Memo. 4, 26pp.

Peixoto, J.P. and A.H. Oort, 1992: Physics of climate, American Institute of Physics, pp. 520.

Schmetz, J. and Q. Liu, 1988: Outgoing longwave radiation and its diurnal variation at regional scales derived from Meteosat. J. Geophys. Res., Vol. 93, D9, 11192 – 11204.

Schmetz, J., C. Geijo, W.P. Menzel, K. Strabala, L. van de Berg, K. Holmlund and S. Tjemkes, 1995: Satellite observations of upper tropospheric relative humidity, clouds and wind field divergence. Contrib. Atmosph. Physics, 68, 345 - 357.

Schmetz, J., S.A. Tjemkes, M. Gube and L. van de Berg, 1997: Monitoring deep convection and convective overshooting with Meteosat. Adv. Space Res., Vol. 9, No. 3, 433-441.

Schmetz, J., P. Pili, S. Tjemkes, D. Just, J. Kerkmann, S. Rota and A. Ratier, 2002: An Introduction to Meteosat Second Generation (MSG). Bull. Amer. Meteor. Soc., 977 – 992.

Soden, B.J., 2000: The diurnal cycle of convection, clouds, and water vapor in the tropical upper troposphere. Geophys. Res. Letters, 27, 2173-2176.

Udelhofen, P.M. and D.L. Hartmann, 1992: Influence of tropical cloud systems on the relative humidity in the upper troposphere, J. Geophys. Res., 100, 7423-7440.